https://doi.org/10.1016/j.conbuildmat.2022.127767

Effects of Seawater on UHPC: Macro and Microstructure Properties

Wing Lun Lam, Peiliang Shen[+], Yamei Cai, Yanjie Sun,
Yangyang Zhang, Chi Sun Poon[*]
Department of Civil and Environmental Engineering, The Hong Kong Polytechnic University, Hung Hom, Kowloon, Hong Kong
+Corresponding author. Email address: peiliang.shen@polyu.edu.hk (P. Shen), * cecspoon@polyu.edu.hk (C.S.Poon)

Abstract

Due to the shortage of fresh water, the use of seawater in concrete production could alleviate the demand for the limited resource. To promote the use of seawater in ultra-high-performance concrete (UHPC), the effects of seawater on the hardening process and the corresponding relationship between the macroscopic performance and hydration, pozzolanic reaction, and microstructure of hydration products were investigated. Earlier setting times, higher early but lower later compressive strength and higher shrinkage of UHPC were observed. The modified performance was not only attributed to the presence of seawater accelerating the early hydration but also due to the change of microstructure and C-S-H structure. Better early strength and exacerbated shrinkage were associated with the slightly reduced porosity but refined pore structure, while lower later-age compressive strength in the seawater group was related to coarser microstructure and shorter mean chain length (MCL) and lower polymerisation of C-S-H. In addition, the pozzolanic reactivity of silica fume was enhanced, which would also contribute to the increased early compressive strength and exacerbated shrinkage of UHPC. It should be noted that no Friedel's salt and brucite were observed in the seawater UHPC. Moreover, although the incorporation of fly ash (PFA) was able to

compensate for the adverse effects of seawater on compressive strength and autogenous shrinkage of UHPC, the exacerbated drying shrinkage was still a concern even when fly ash was present.

Keywords: UHPC; Seawater; Microstructure; Pozzolanic reaction; Silica fume; Shrinkage

1. Introduction

The consumption of concrete for infrastructure has been increasing in countries with rapid development. The production of concrete has estimated to reach 30 billion tonnes worldwide [1]. Natural resources such as freshwater for concrete production has also been in a very high demand [2]. For instance, freshwater shortage and transportation costs have been great concerns in construction of marine environment, remote areas, and offshore islands. As an alternative to freshwater, the use of seawater in concrete has attracted increasing attention to address the shortage and economic issues in conventional concrete production [3-5].

To promote the use of seawater in concrete production, the effect of seawater on the properties of concrete has been widely studied. Incorporating seawater in concrete could increase the early hydration rate and cumulative heat compared to conventional concrete [6, 7]. As a result, a denser microstructure at early age was usually observed in seawater concrete due to the formation of more hydrates [8-10]. Compared to normal strength concrete prepared with fresh water, a newly generated hydrate, Friedel's salt, could be observed in seawater mixed concrete due to the reaction of C_3A and chloride ion in seawater[6, 7, 11, 12].

The advantages and disadvantages of seawater on the performance of concrete have also been identified. One of the advantages of incorporating seawater in concrete can

be demonstrated in the improvement of early age mechanical properties. The early compressive strength up to 7 d can be improved, while the compressive strength at 28 d is comparable to conventional concrete[4]. However, the disadvantages can be illustrated in fresh properties and durability. The incorporation of seawater shortened setting time due to the accelerated hydration [10, 13]. Although seawater can adversely affect fresh properties of concrete, the effect can be considered as minimal [4]. Moreover, seawater can also lead to increased drying shrinkage which can result in cracking, and incorporating supplementary cementitious materials (SCMs) in seawater concrete has been suggested to minimize drying shrinkage [10]. The risk of steel corrosion due to the presence of chloride is also the main concern for the use of seawater[14]. However, because of the proposed incorporation of fibre-reinforced polymer (FRP) in seawater concrete, steel corrosion is no longer a concern [15, 16]. Based on the effect of seawater on concrete properties, seawater concrete could be a feasible solution as an environmentally friendly material in construction to address the shortage of natural resources for concrete production.

UHPC is an advanced cement-based material which was developed in 1990s[17]. The characteristics of UHPC include using a low water to binder ratio, high cement content, large amount of silica fume as well as no coarse aggregate, leading to differences in performance and hydration from normal concrete. For instance, UHPC possesses excellent mechanical (compressive strength > 120 MPa according to ATSM C1856/C1856M[18]) and durability properties, denser microstructure [19, 20] and a small amount of calcium hydroxide (CH) [21] in its matrix. Thus, compared to conventional concrete, these unique features might lead to different effects when using seawater as the mixing water in UHPC. Our recent study regarding the corrosion behaviour of cement paste and UHPC paste mixed with seawater supported this

argument. The study showed that propagation of steel corrosion was observed in the normal cement paste mixed with seawater, which was attributed to insufficient OH^- concentration in pore solution, which is the key factor that can produce a strong passivation film to inhibit the corrosion process [22]. However, the corrosion behaviour was different in seawater mixed UHPC. The corrosion of steel was only induced in seawater mixed UHPC initially, but it was suppressed within the first few days, resulting from the deficiency of water and oxygen [22]. These variations in corrosion of steel reinforcement were attributed to the different effects of seawater on the microstructure and hydrates on UHPC.

Moreover, SCMs, such as silica fume and pulverised fly ash (PFA), can further enhance the applicability of UHPC by promoting sustainability and improving the properties of UHPC. In UHPC, due to the characteristics of low water to binder ratio, most of the cementitious material remains unhydrated and acts as an inert filler. Silica fume and PFA, as a by-product, can therefore play an important to substitute the cementitious material as the inert filler in order to lower carbon green footprint in UHPC production [23]. Moreover, PFA can improve workability, reduce water absorption and minimize shrinkage [23-25]. However, previous studies did not well investigate the effect of seawater on the pozzolanic reaction of SCMs in UHPC [26].

In UHPC production, the lack of fresh water is undoubtedly also one of the challenges. To promote the application of seawater in UHPC, Teng et.al [27] reported a slight reduction in workability, density and modulus of elasticity of UHPC incorporating with seawater, while the early compressive strength increased up to 7 days and decreased afterwards. Dong et.al [28] studied the flexural behaviour of UHPC incorporating coral aggregate and seawater and found that the ultimate bending capacity was improved. Huang et.al [29] studied the mechanical performance and cracking behaviour of UHPC

mixed with seawater. Li et.al [30] studied the shrinkage behaviour of cement and silica fume paste at water to binder ratio of 0.2 and showed a reduction in autogenous shrinkage when mixing with seawater. These previous studies mainly focused on the performance or engineering aspects of UHPC prepared with seawater. The understanding of the effect of seawater on hydration, microstructure, and hydration products of UHPC is still limited. The underlying mechanism controlling the evolution of macroscopic properties of UHPC incorporating with seawater is also unknown.

Therefore, this study focused on evaluating the effect of seawater on the hydration, macroscopic properties, and microstructure of UHPC, aiming to obtain the microstructure and hydration products evolution of UHPC and understand the hardening process. Correlation between the macroscopic properties, with the hydration, microstructure of the hydration products of UHPC was revealed.

2. Materials and experimental methods

2.1 Materials

In this study, the binder of the UHPC was produced from ASTM type I ordinary Portland cement (OPC, 52.5) and a commercially sourced silica fume (Elkem). ASTM Class F fly ash (PFA) sourced from a local power company was also used as a SCM. The chemical compositions of the cementitious materials determined by X-ray Fluorescence Spectrometer (XRF) (Supermin 200, Rangaku Corporation, Japan) are shown in Table *1*. The particle size distributions of the materials determined by a laser diffraction particle size 144 analyser (Malvern Mastersizer 3000E) are shown in Fig. *1*(a). Two types of mixing water, tap water and an artificial seawater specified by ASTM D1141-98 [31], were used. The compositions of the artificial seawater are shown in Table *2*. River sand with a size ranging from 0.15 to 2.36 mm was used as the fine aggregate. A Polycarboxylate ether (PCE) superplasticizer (BASF) with a specific

gravity 1.05 was used. Copper coated straight steel fibre with a diameter of 0.22mm and a length of 13mm was also incorporated in the UHPC mixtures.

Table 1 Chemical compositions of the cementitious materials (%)

Compositions	SiO_2	CaO	Fe_2O_3	MgO	SO_3	Al_2O_3	K_2O	Na_2O	P_2O_5
OPC	19.1	65.2	2.96	0.754	4.27	6.06	0.684	0	0.138
Silica fume	95.7	0.729	0.0733	0.714	0.274	0.446	1.74	0	0.087
PFA	37.0	14.0	10.9	5.50	2.61	22.9	1.37	3.75	0.528

OPC: Ordinary Portland Cement; PFA: fly ash; GGBS: ground granulated blast-furnace slag

Table 2 Compositions of the artificial seawater

Compositions	NaCl	$MgCl_2$	Na_2SO_4	$CaCl_2$	KCl	$NaHCO_3$	KBr
Concentration(g/L)	24.5	5.20	4.09	1.16	0.695	0.201	0.101

2.2 Methodology

2.2.1 Specimen preparation

The mixture proportion of UHPC (Table *3*) was obtained based on the modified Andreasen and Andersen model to optimize the packing of the binder and river sand [32]. In the modified Andreasen and Andersen model, the volume proportion of cement, silica fume and PFA can be optimized by using the Least Squares Method with a partition coefficient to minimize the target grading curve and the mix. A partition coefficient of 0.23 was used in this study. Two types of mixture, called the control group (CON) and fly ash group (FA), were prepared using the simulated seawater and tap water as mixing water. The cumulative volume of cement, silica fume, PFA and river sand, and the optimal grading curves of the design mixture is shown in Fig. *1*.

In this study, paste, concrete and fibre reinforced UHPC specimens were prepared for different tests. To prepare the paste specimens, the binders, such as cement, silica fume and PFA, were prepared according to Table *3* (without sand and steel fibre) and dry

mixed at low speed for three minutes by using a pan mixer. Water and superplasticizer were then added into the mixer and mixed with the binders for 2 minutes at low speed and subsequently 3 minutes at high speed. After that, 1- minute low-speed mixing was applied to remove the bubble produced from high-speed mixing. For the concrete specimens, river sand was added into the fresh mixed paste and mixed in the mixer for 2 minutes at high speed, followed by 1 minute at low-speed mixing. It should be noted that 2% steel fibre by volume was added in the specimens for compressive strength, autogenous and drying shrinkage tests. For the fibre reinforced UHPC specimens, 2% steel fibre by volume was also added together with river sand before the 2-minute high-speed mixing and 1-minute low-speed mixing. After the mixing process, the paste, concrete or fibre reinforced specimens were respectively vibrated on a vibration table for 1 minute to remove entrapped air.

Table 3 Mixture proportions of the UHPC mixtures

Compositions (kg/m^3)	FC	SC	FF	SF
Cement	902	902	820	820
Silica fume	246	246	246	246
PFA	0	0	82	82
River Sand	920	920	920	920
Tap water	156.13	---	156.13	---
Seawater	---	156.13	---	156.13
PCE Superplasticizer	34.44	34.44	34.44	34.44
Steel fibre (2% in volume)	156	156	156	156

FC: CON group mixed with fresh water; SC: CON group mixed with seawater; FF: FA group mixed with fresh water; SF: FA group mixed with seawater

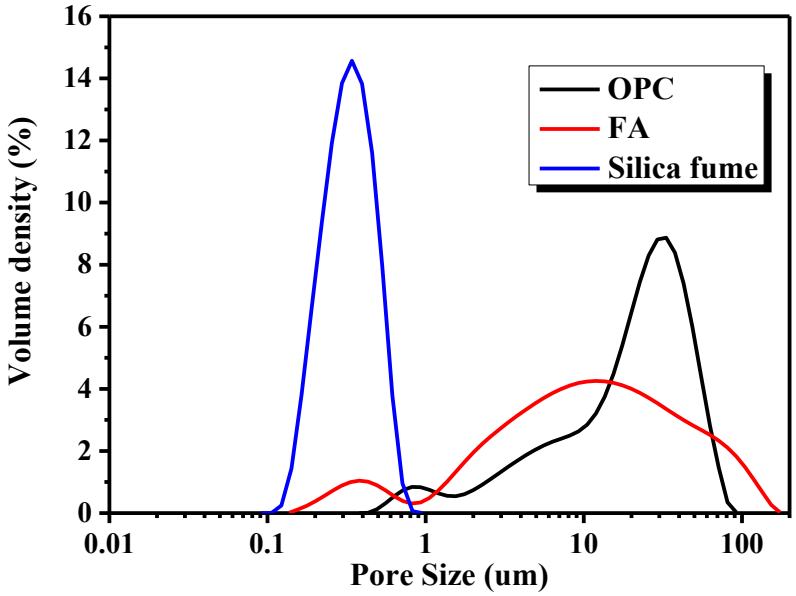

(a)

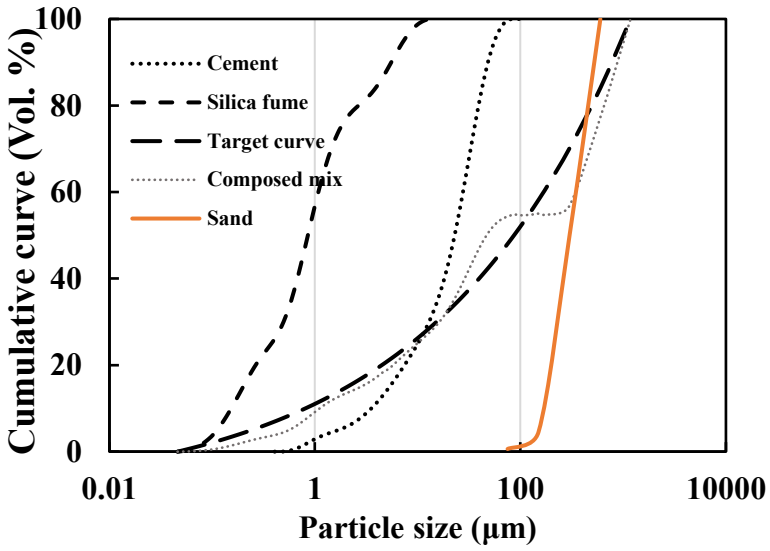

(b)

159 Fig. 1 (a) Particle size distributions of cementitious material and (b) cumulative curve and the optimal grading curve
160 design

161 *2.2.2 Compressive Strength*

162 The fibre reinforced specimens with the size of 40 mm × 40 mm × 160 mm were cast
163 in steel moulds to determine the compressive strength of UHPC. The specimens were

sealed with plastic wraps immediately after casting and demolded at 24h. The specimens were then cured in tap water at 25 ± 1 ^{o}C until the testing ages. The compressive strength was obtained from three specimens at 1, 7 and 28 days respectively with the loading rate of 0.9 kN/s.

2.2.3 Slump flow & setting time

The procedure used for slump flow followed BS EN1015-3 [33]. The test was conducted for the concrete specimens immediately after the mixing process. Penetration resistance test was also performed on concrete specimens based on ASTM C403 - 08 to obtain the setting time [34]. A penetration resistance apparatus with an appropriate needle size selected based on the degree of setting was used to measure the penetration resistance produced from the 25mm penetration of the corresponding needle. To prepare the specimen, each specimen was cast in a cylindric container with a diameter and depth of 150 mm and sealed with plastic wraps immediately after casting. The specimens were then stored in an environmental chamber at 23°C ± 2 °C prior to the testing. The initial test was performed at 2 hr after casting, and the subsequent tests were conducted at ½ hr intervals. It should be noted that the time intervals were adjusted to obtain sufficient results (at least 6 penetrations). The initial setting and final setting of the concrete specimens were determined at the time when the penetration value reached 2.5MPa and 27.6MPa respectively in the plot of penetration resistant – elapsed time curve[34].

2.2.4 Autogenous shrinkage & drying shrinkage

The autogenous shrinkage of the fibre reinforced specimens was determined according to ASTM C1698-19 [35]. The duration of the test was 7 days and the frequency of data collection for the UHPC autogenous shrinkage strain was once in each hour in the first day, and twice a day for the rest of the time.

The test procedure of drying shrinkage of the fibre reinforced specimens was based on a modified British Standard (BS ISO-Part 8, 2009) [36]. The specimens were cast in steel moulds with the size of 25 mm × 25 mm × 285 mm and sealed with plastic wraps for 24h. The specimens were then demolded and cured in water for 48 h. After curing, the specimens were transferred to and cured in environmental chamber at 25°C ± 2 °C with a relative humidity of 50% ± 4%. The drying shrinkage strain was tested at 4, 7, 14, 28 and 56 d.

2.2.5 Heat of hydration

The heat flow and cumulative heat of the paste (without aggregate and fibre) of UHPC specimens were obtained using an I-Cal 4000 isothermal calorimeter. Approximately 50g UHPC pastes prepared according to Table *3* were prepared and placed in plastic containers. After 15 minutes of hand mixing the specimens were placed into the calorimeter for the heat flow measurement.

2.2.6 Pore Structure

To obtain the pore structure with the size between 2nm to 200nm, the nitrogen adsorption and desorption isotherms of the UHPC were determined by Tristar 3020, Micromeritics. The samples were fractured into small pieces with the size of less than 1mm from the paste specimen. The hydration of samples was stopped at age 1 and 28 d by soaking in ethanol, followed by being dried for 48h in a vacuum oven at 45ºC.

2.2.7 Characterization of the evolution of hydration products

The hydration of the samples was stopped at ages 1, 7 and 28 d by soaking in ethanol. The paste samples were then prepared as dry powder with size less than 45 μm and analysed by X-ray diffraction (XRD) with Cu-Kα radiation where λ = 1.54 Å operated at conditions of 45kV and 200mA. The measurement was recorded with a range of 5-

80° 2θ with a step size of 0.02◦. The XRD spectra were analysed by MDI Jade 6.5 software.

2.2.8 Nuclear Magnetic Resonance spectroscopy (NMR)

The mean chain length (MCL) and polymerization degree (PD) of C-S-H and the hydration degree (HD) of the 28 d specimens were studied to explain the result of compressive strength, via the scanning of ^{29}Si nuclei by a JEOL ECZ 500 MHZ solid-state NMR spectrometer with a 7-mm CP/MAS probe. Approximately 1g powdered paste samples were prepared according to the TGA procedures and were analysed for the NMR test. The solid state ^{29}Si NMR spectra of the nuclei were obtained under the conditions of 4kHz spinning rate, 98.4MHz resonance frequency and 20s relaxation delay. The spectra were deconvoluted and analysed according to Q^n classification [37] (where Q refers to silica tetrahedra (SiO_4) and n refers to different types of silica tetrahedra) to obtain mean chain length (MCL) and polymerization degree (PD) . The following are the equations of MCL and PD.

$$MCL = 2 \times (Q^1 + Q^2) / Q^1 \quad (1)$$

$$PD = Q^2 / Q^1 \quad (2)$$

2.2.9 Pozzolanic reactivity of silica fume

The 7-d pozzolanic reactivity of silica fume in seawater was studied by isothermal calorimetry (I-Cal 4000 isothermal calorimeter) and thermogravimetric analysis (TG; Rigaku Thermo Plus EVO2). The samples were prepared based on the modified procedures of the previous study [38]. Since seawater can react with potassium hydroxide solution and form precipitate during the preparation, silica fume was only blended with reagent grade CH in a mass ratio of 1:3. A portion of the blend without mixing water was reserved for TG analysis to determine the CH content in the unhydrated blend. The rest were mixed with tap water or seawater at a liquid to solid

ratio of 0.63. PCE was also added at a PCE to silica fume ratio of 0.14. The mass ratio of silica fume, water and PCE was determined based on the mix proportions of Table *3*. After mixing, the samples were cured in a sealed plastic container and stored in an environmental chamber at a temperature 25°C ± 1 °C for 7 d. The samples were then soaked in isopropanol for 3 days to stop the pozzolanic reaction, followed by vacuum drying at 40°C for 6 hr. 10 mg of the samples were ground into powder and heated from 30°C to 1000°C at a rate of 10°C/min in N_2 environment using a Rigaku Thermo Plus EVO2. For isothermal calorimetry, tap water and seawater blends were prepared to measure the heat flow measurements for 7 d.

3. Results

3.1 Evolution of fresh properties of UHPC containing seawater

Regarding the fresh properties, setting time and slump of seawater and tap water group were shown in Table *4*. In CON, the initial and final setting time in the seawater group were approximately 50% shorter than the tap water group. The initial and final setting time were also reduced in FA group but with less extent of 25%. The shortened setting time was attributed to the accelerated hydration [7]. Similarly, the initial and final setting times of the seawater concrete were also shortened due to the presence of seawater shown in Table *4*. Regarding the slump flow, although the slump flow of the seawater mixed specimens was about 10 mm higher than that of tap water mixed specimens, the result was comparable. Furthermore, for FA group, the higher slump flow was observed compared to CON group. The observation was related to spherical shape of PFA acting as a lubricant between the binder particles [39]

Table 4 Fresh properties of UHPC and cement paste

	FC	SC	FF	SF

Initial Setting(min)	315	205	330	280
Final Setting(min)	375	240	400	315
Slump(mm)	210	220	220	230

TW: tap water; SW: seawater

3.2 Mechanical properties of UHPC incorporated with seawater

Fig. *2* shows the compressive strength results. In the CON group, the compressive strength of the specimens prepared with seawater was higher than that of the samples mixed with tap water at 1 d and the difference was approximately 5 MPa. However, UHPC mixed with tap water attained a higher compressive strength after 7 d. It was approximately 10 MPa higher than the samples prepared with seawater at 28 d. The trend of strength development was consistent with previous studies [4, 27]. For the FA groups, the seawater sample had a slightly higher compressive strength at 1 d. However, at 7 d and 28 d, seawater showed limited influences on the compressive strength as similar compressive strength was observed.

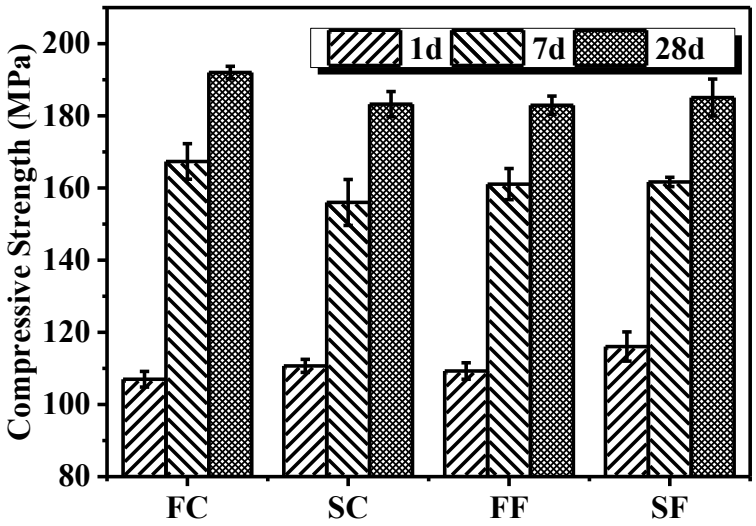

Fig. 2 Compressive strength of UHPC at 1, 7 and 28d

3.3 Volume stability of UHPC prepared with seawater

The autogenous shrinkage test results are shown in Fig. *3*. In CON group, 7 d-autogenous shrinkage the samples mixed of seawater reached approximately 1,100 × 10^{-6}, which was 500 × 10^{-6} higher than the sample that mixed with tap water. The result was contradicted to previous study[30]. When the PFA was incorporated in UHPC, the autogenous shrinkage of both groups showed a decrease. The autogenous shrinkage was reduced by 27% and 23% in the seawater mixed and tap water mixed samples respectively, which was attributed to the replacement of cement by PFA [40, 41]. Indeed, the autogenous shrinkage of the seawater mixed sample, even with the incorporation of PFA, was higher than tap water mixed samples.

Fig. *4* illustrates the drying shrinkage of the UHPC samples. Similar to that of the autogenous shrinkage test, the UHPC prepared with seawater induced higher shrinkage compared with the tap water group.

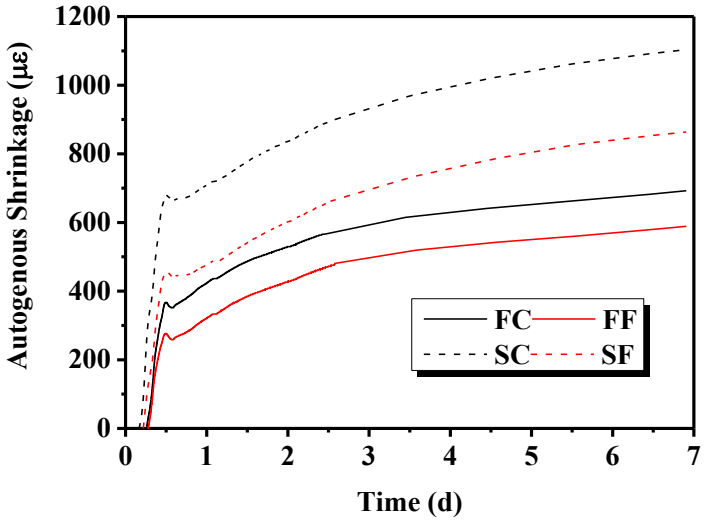

Fig. 3 Effect of seawater on autogenous shrinkage of UHPC

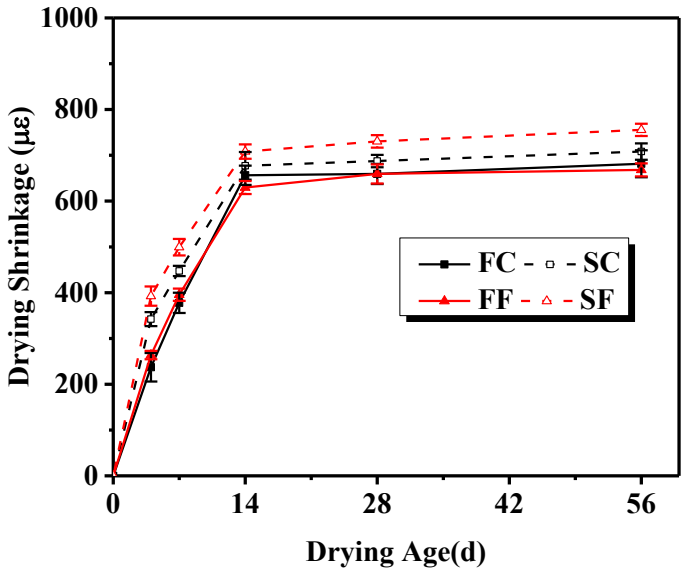

287

288 Fig. 4 Effect of seawater on drying Shrinkage of UHPC

289 *3.4 Hydration and hydration products of UHPC prepared with seawater*

290 Fig. *5*(a) illustrates the heat flow curves of UHPC mixed with seawater and tap water
291 up to 40 h. The dormant period was approximately 2.5 h shorter in the seawater group
292 compared with the tap water group. The peaks in the seawater group also occurred 2 h
293 earlier and were approximately 0.2mW/g higher than that in the tap water group.
294 Regarding the cumulative heat curves shown in Fig. *5*(b), the amount of cumulative
295 heat of the seawater group also was evidently higher than the tap water group up to 40h.
296 The result showed seawater promote the hydration of UHPC paste which was attributed
297 to the presence of seawater ions, including Cl^-, Ca^{2+}, Mg^{2+}, Na^+ and SO_4^{2-} accelerating
298 the hydration of C_3A and C_3S [42, 43].

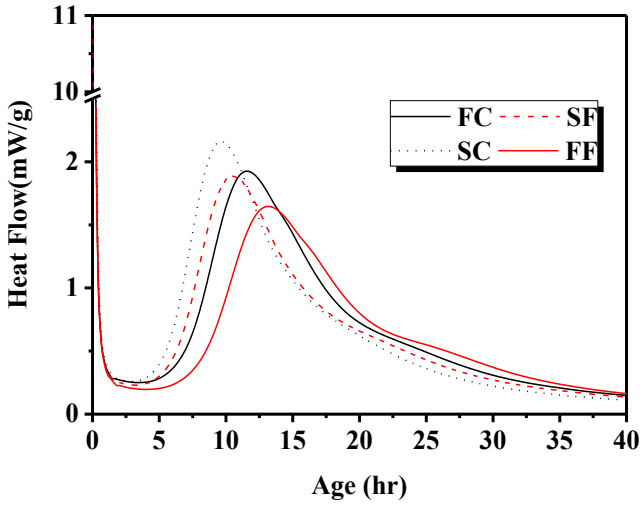

(a) Heat Flow

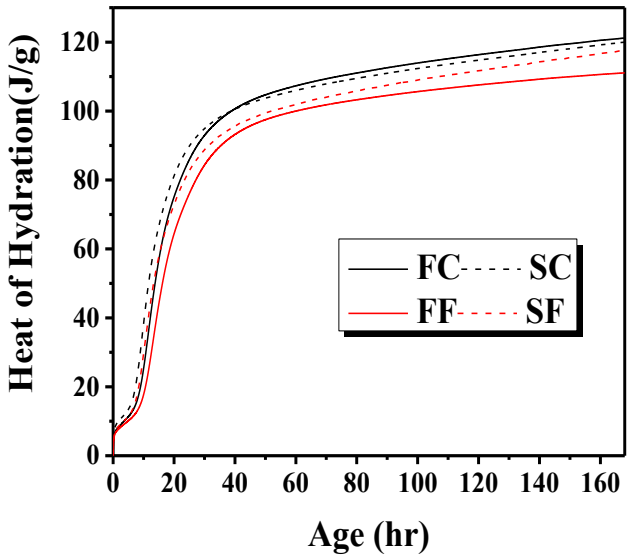

(b) Cumulative Heat

299 Fig. 5 (a)Heat Flow and (b) Cumulative heat of UHPC mixed with tap water and seawater

300 To understand the modification of C-S-H structure due to the presence of seawater, ^{29}Si
301 MAS-NMR was conducted. Fig. *6* shows the ^{29}Si MAS-NMR spectra and the
302 deconvoluted peaks of UHPC mixed with tap water and seawater at 28d. Four silica
303 tetrahedra (SiO_4) peaks were observed in all groups at all ages. The peaks of Q^0 (-
304 72ppm), Q^1 (-81 ppm), Q^2(-86ppm) and Q^4 refer to SiO_4 in cement, bridging SiO_4 in C-

S-H, the end-chain SiO_4 in C-S-H and SiO_4 in PFA and silica fume respectively [44]. Table *5* shows the ^{29}Si MAS NMR spectrum analysis of the UHPC mixed with tap water and seawater at 28 d. The MCL and PD in seawater group at 28d were both lower than tap water group.

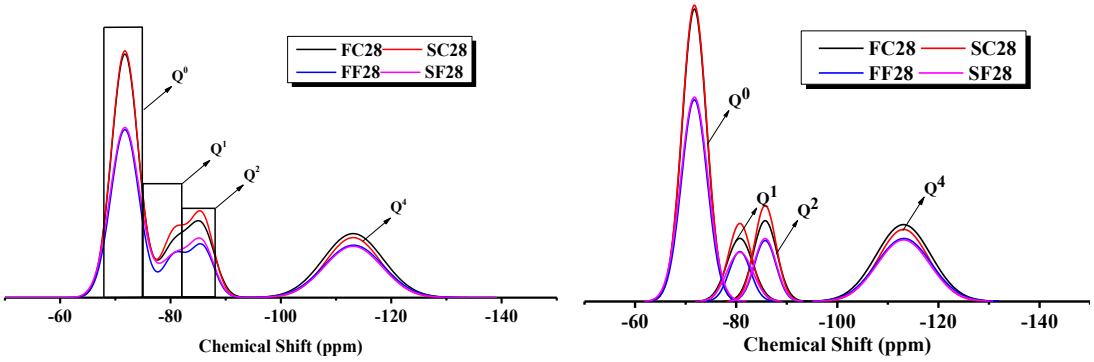

(a) ^{29}Si MAS-NMR spectrum at 28d (b) deconvoluted peaks 28d

Fig. 6 ^{29}Si MAS-NMR spectra and deconvoluted peaks of UHPC mixed with tap water and seawater at 1d and 28d

Table 5 ^{29}Si MAS NMR spectrum analysis of UHPC mixed with tap water and seawater at 28 d

	Q^n/%				MCL	PD
	Q^0	Q^1	Q^2	Q^4		
FC28	47.62	10.31	14.18	27.89	4.75	1.38
SC28	49.40	12.12	14.01	24.47	4.31	1.16
FF28	47.11	9.73	11.89	31.27	4.44	1.22
SF28	48.51	11.10	12.10	28.30	4.18	1.09

The results of XRD are shown in Fig. *7*. It was surprising to note that no significant difference was observed in the crystalline hydration products of UHPC samples. The formation of Friedel's salt and brucite were expected in the seawater mixed specimens since several studies on seawater concrete detected the Friedel's salt through XRD or TG analysis [45, 46]

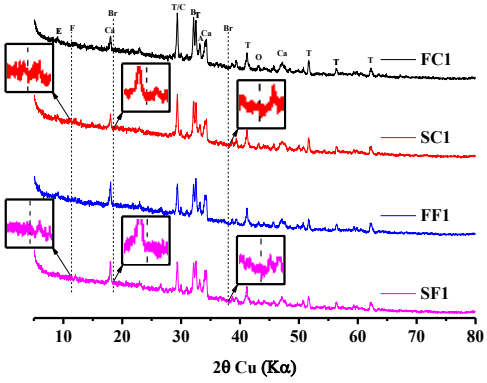

a) XRD at 1d

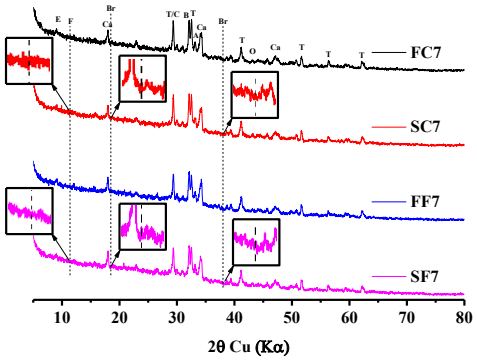

b) XRD at 7d

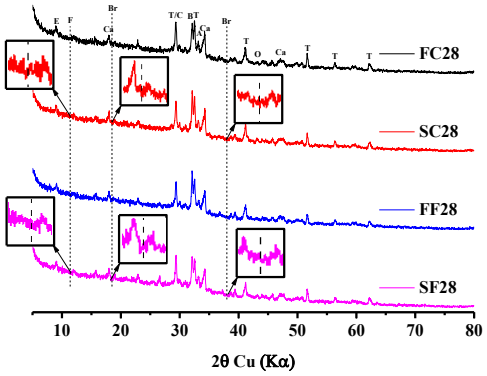

c) XRD at 28d

Fig. 7 XRD spectrum of UHPC mixed with tap water and seawater at 1, 7& 28d (E = Ettringite; F = Friedel's salt; Ca = $Ca(OH)_2$; Br = $Mg(OH)_2$; T = C_3S; C = Calcite; B = C_2S; A = C_3A; O = Al_2O_3)

3.5 Pore structure evolution of UHPC prepared with seawater

The pore structures determined by BET are shown in Fig. *8*. The total pore volume of the seawater and tap water samples at 1 d were comparable. However, in the samples prepared without PFA, the volumes of pores larger than 50nm and less than 50nm in SC and FC was 0.0250mL/g and 0.0256 mL/g, and 0.0249 mL/g and 0.0246 mL/g respectively. Therefore, seawater indeed promoted the formation of a denser microstructure of UHPC at 1 d as SC had more finer pores than FC. According to the pore structure at 28 d, seawater did not refine the pore structure as in 1 d. 0.0244 mL/g and 0.0234 mL/g of pore volume larger than 50nm and 0.008 mL/g and 0.0102 mL/g

pore volume less than 50nm were observed in SC and FC at 28 d respectively. SC therefore had a coarser microstructure than FC at 28 d. The result showed seawater refined the pore structure at the early age but coarsened the pore structure at the later age. However, the results in the samples prepared with PFA was in the contrary. SF had less coarser pores and a denser microstructure, and therefore a higher compressive strength than FF.

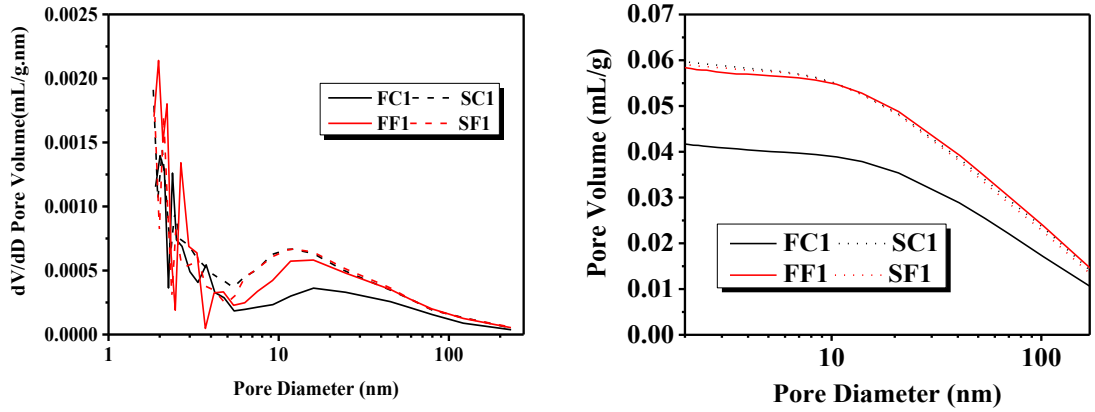

(a) dV/dD Pore Volume of UHPC at 1 d (b) Cumulative pore volume at 1 d

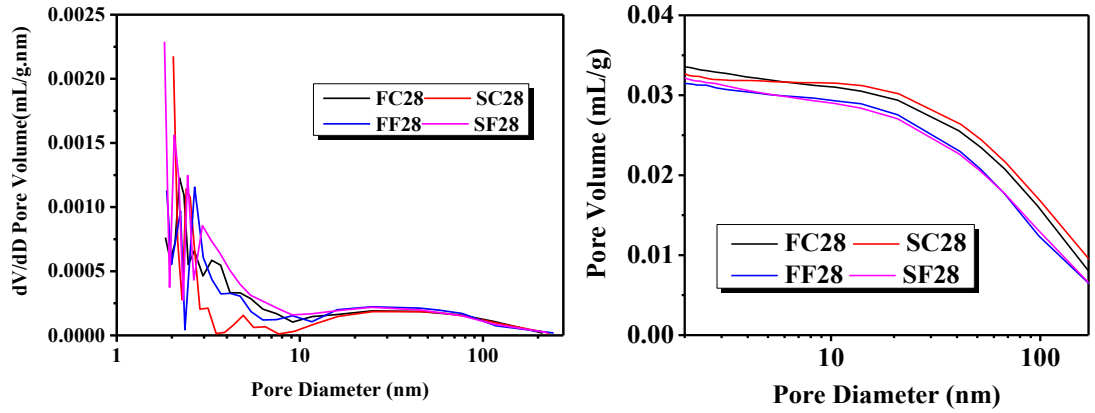

(c) dV/dD Pore Volume of CON at 28 d (d) Cumulative pore volume at 28 d

Fig. 8 dV/dD Pore Volume and cumulative pore volume of UHPC mixed with seawater and tap water

3.6 Pozzolanic reactivity of silica fume

Fig. *9*(a) shows the TG and DTG curves of silica fume and CH blends mixed with tap water and seawater and cured for 7d. In DTG, several mass loss peaks can be observed

in UHPC. The first peak occurred around 100 to 200 °C was due to the mass loss of free water and physically water bound on hydrates such as C-S-H [44, 47]. The peak around 450 °C was attributed to dehydroxylation of $Ca(OH)_2$ [48]. The blend mixed with seawater had evidently a higher peak intensity of C-S-H than the corresponding sample mixed with tap water. The CH peak in the seawater mixed samples was also higher than that in the tap water mixed sample. Fig. *9*(b) compares the cumulative heat evolved from the blends. The seawater sample had a higher cumulative heat during the whole testing period. The cumulative heat evolved is plotted against the amount of CH consumed by the silica fume in Fig. *9*(c). After 7 d, the cumulative amounts of heat released by the seawater sample and tap water sample were 227.8 J/g SCM and 168.3 J/g SCM respectively. The seawater sample released 26% more heat than the tap water sample. The seawater mixed sample also recorded approximately 30% higher CH consumption than the tap water mixed sample after 7d of curing. The higher amount of C-S-H formation, CH consumption, and cumulative heat evolved provided strong evidence that seawater enhanced the pozzolanic reaction of silica fume in UHPC[38]. The enhanced pozzolanic reactivity of silica fume could be attributed to the high solubility of CH in seawater[49], leading to more dissolved ions for pozzolanic reaction.

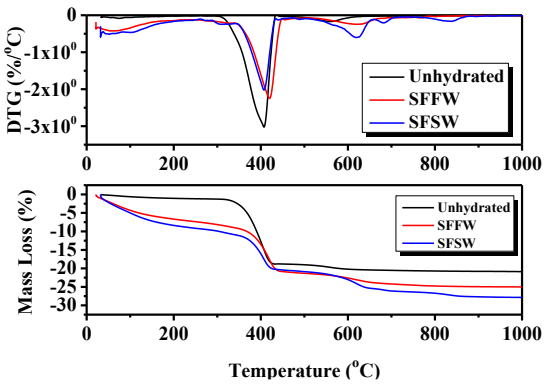

(a)

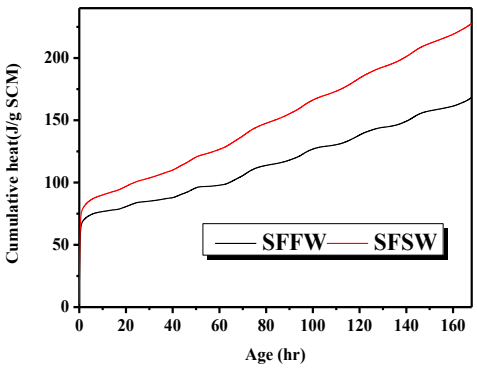

(b)

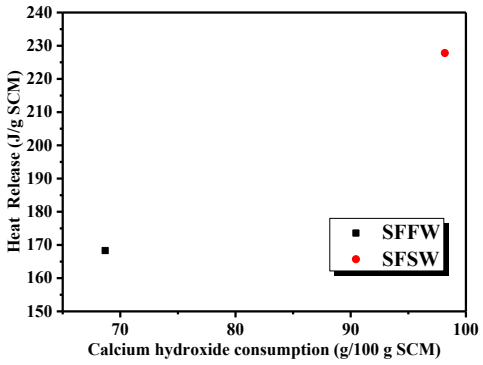

(c)

Fig. 9 a) TG and DTG curve of CH and silica fume mixed with tap water and seawater at 7d; b) CH consumption by silica fume mixed with tap water and seawater at 7d; c) cumulative heat against calcium hydroxide consumption for silica fume mixed with tap water and seawater (note: Unhydrated: silica fume mixed with CH without mixing water; SFFW: silica fume mixed with tap water; SFSW: silica fume mixed with seawater)

4. Discussion

4.1 Effect of seawater on fresh properties

The initial and final setting time were shortened due to the presence of seawater. The role of seawater in shortening setting was related to the accelerated hydration. Particularly, the process of dissolution of cement particles and nucleation of hydrates was accelerated in Fig. *5*(a). The ions of seawater accelerated the process of dissolution of cement particles [6, 7] and nucleation process [50], eventually leading to shortened initial and final setting times. While incorporating PFA in UHPC, prolonged initial and final setting times were observed in FA group since the retardation of hydration was reported due to the presence of PFA[51].

4.2 Effect of seawater on hardening process

An increase in early compressive strength was observed which was certainly related to hydration and microstructure. However, since a high amount of SCMs was incorporated into the UHPC, the pozzolanic reaction could also affect the compressive strength.

1) Improved early hydration degree

Firstly, the improved early strength can be explained in the aspect of hydration. Since seawater accelerated the hydration, the higher degree of hydration and more C-S-H formation were observed in the seawater mixed samples [7, 52], resulting higher compressive strength.

2) Refinement of pore structure at early age

Secondly, regarding the pore structure, although the total porosity was similar, the accelerated hydration due to seawater promoted a denser microstructure of UHPC resulting in higher early compressive strength. Particularly, the pores larger than 50nm was associated with compressive strength [53, 54]. According to Fig. *8*, in the samples prepared without PFA, although the total pore volume of the seawater and tap water samples at 1 d were comparable, the seawater group had fewer pores larger than 50nm. While in the samples prepared with PFA, a lesser volume of pores greater than 50nm were also observed in the seawater mixed sample and the total porosity of the seawater mixed sample was evidently lower than the tap water mixed sample. As a result, a denser microstructure was observed in the seawater samples prepared with or without PFA and contributed to the higher compressive strength.

3) Enhanced pozzolanic reaction of silica fume

Thirdly, the improved early strength might also be associated with the increased pozzolanicity of silica fume due to the presence of seawater. More C-S-H was formed by the pozzolanic reaction of silica fume in the seawater samples. The improved early strength might also be associated with the accelerated hydration of cement by seawater. Increased formation of $Ca(OH)_2$ was reported due to the accelerated hydration by seawater [49]. The y increased CH concentration could facilitate the pozzolanic reaction of silica fume and therefore a better early compressive strength was observed.

In addition, at the later age, the compressive strength was reduced when seawater was used as the mixing water. The reduced performance was due to different hardening process as discussed below.

1) Coarsened pore structure at later age

According to the pore structure at 28 d, although FC and SC had a similar total porosity, a higher volume of coarser pores was observed in SC. However, the results for the sample prepared with PFA were contrary. SF had less coarser pores and a denser microstructure, and therefore a higher compressive strength than FF. The result showed seawater might refine the pore structure of UHPC prepared with the incorporation of PFA.

2) Reduced polymerization of C-S-H at later age

In addition, the modification of C-S-H structure due to seawater was associated with the reduced later compressive strength in SC. The decrease of mean chain length (MCL) and polymerisation degree (PD) of C-S-H was observed in a previous study due to the presence of seawater ions, such as Na^{+} and Mg^{2+} [45, 55]. These ions could inhibit the polymerisation of C-S-H by the substitution of the Ca^{2+} in the interlayer of the C-S-H structure, especially for low Ca/Si C-S-H [45]. C-S-H formed by fly ash or silica fume have typically lower Ca/Si ratios and therefore could be sensitive to the inhibition of C-S-H polymerisation. The effect of MCL and PD on compressive strength had been reported [56].

In summary, the mechanical performance of seawater UHPC was not only influenced by effect of accelerated hydration, but also the modification of the pore structure and C-S-H structure. Although seawater promoted the increased hydration degree of UHPC, which was confirmed to contribute to the increased mechanical properties initially, the

adverse effect of coarsened pore structure and shortened MCL of C-S-H outweighed the positive effect of accelerated hydration.

4.3 Effect of seawater on volume stability

The presence of seawater resulted in higher shrinkage of UHPC, particularly the autogenous shrinkage, causing higher drying shrinkage at the later age. The autogenous shrinkage was highly related to the reaction of the binders with water and the pore structure, which were modified by the presence of seawater [7]. The effect of modified reactions and pore structure on volume stability of UHPC is discussed as follows.

1) Accelerated hydration and pozzolanic reaction

The increased shrinkage was associated with accelerated hydration in the early age due to the use of seawater[57]. The accelerated hydration resulted in a higher degree of hydration and a higher consumption of free water, which therefore lower the relative humidity in the fine pore structure. This could lead to a higher self-desiccation and therefore a higher autogenous shrinkage was observed [9, 30]. Apart from hydration, the pozzolanic reaction of silica fume was also increased because of seawater. The increased pozzolanic reaction could also lead to larger consumption of free water [58] and therefore the autogenous shrinkage could be further increased.

2) Refined pore structure at early age

The higher autogenous shrinkage was also associated with the pore size distribution modified by seawater. According to the pore size distribution in Fig. *8*, more pores in the size range of less than 50nm were observed in the seawater mixed sample at 1 d and this was also associated with autogenous shrinkage[53, 54, 59]. This size range of pores mainly contributed to shrinkage as capillary pressure was higher with the smaller pore [60].

Shrinkage was an important issue in UHPC that led to durability concerns [61, 62], while the exacerbation of shrinkage due to seawater might not favour the use of UHPC with seawater. The conventional measures to reduce the shrinkage was by incorporating PFA and this measure might no longer be effective as well in mixes prepared with seawater.

4.4 Comparison with normal strength concrete

Compared to normal concrete, UHPC was characterized by an ultra-low water to binder ratio, high content of superfine powders and no coarse aggregate, leading to a dense microstructure and ultra-high performance in terms of mechanical and durability. These different characteristics would affect the role of seawater on the performance and microstructure and hydration products in concrete. The main differences are summarized as follows:

1) Shortened difference of initial and final setting time

For fresh properties, based on previous published literature shown in Table *6*, although the setting time of normal concrete was also shortened, the effect of seawater on setting time of UHPC was more significant than that in normal concrete. The shortening of setting time of UHPC was 20% higher. The reason for the observation was possibly related to the incorporation of silica fume in UHPC since seawater also enhanced the pozzolanic reaction of silica fume in UHPC.

Table 6 Difference of setting time between UHPC and conventional concrete

	Initial set(min)	**Final set(min)**
FC	315	375
SC	205	240
Difference (%)	53.6%	56.3%

TW mixed normal concrete [13]	150	397
SW mixed normal concrete [13]	114	310
Difference (%)	31.5%	28.1%

TW: tap water; SW: seawater

2) Similar compressive strength development but unchanged porosity

The effect of seawater on the compressive strength of UHPC and normal strength concrete was similar. Seawater would accelerate the hydration and promote the early strength development of both UHPC and normal strength concrete at 1 d but then the strength development would be reduced afterwards [10]. However, regarding porosity, this study did not observe significant difference in the seawater UHPC, but the porosity in seawater normal concrete was reduced[10].

3) Increased drying shrinkage and autogenous shrinkage

When comparing the drying shrinkage of the seawater mixed UHPC and normal strength concrete, the results showed the increased drying shrinkage was also observed in the seawater mixed normal strength concrete and this was attributed to the more fine pores in the microstructure[4, 10, 57, 63].

However, the result of autogenous shrinkage in normal concrete was different to UHPC. A study showed a decrease in autogenous shrinkage in an OPC paste prepared with a 0.45 of water to cement ratio and attributed to the thermal expansion due to the accelerated hydration and the restraint by rapid formation of ettringite [6].

The incorporation of PFA was partially useful for controlling the volumetric change of concrete. The PFA reduced the autogenous shrinkage regardless of the type of mixing water used [57]. However, the drying shrinkage reducing effect by using PFA was less effective according to this study. This might suggest seawater concrete could be a concern in terms of shrinkage.

4) Absence of Friedel's salt in UHPC

It is also noted that Friedel's salt was not observed in UHPC at all ages according to Fig. *7*, while it could be observed in normal strength concrete. Lollini et al. [64] attributed this observation to the poor reaction of the alumina phases in cement to form Friedel's salt at a low w/b. The absence of Friedel's salt in this study might also be related to the presence of a large amount of silica fume [65]. Li et.al [30] also suggested the dissolution of C_3S and C_3A enhanced the reaction of silica fume and cement resulting in enhanced formation of C-S-H for physical binding of chloride. The free chloride available for the formation of Friedel's salt would be reduced. However, the effect of Friedel's salts on UHPC performance and normal concrete is still unknown.

5. Conclusion

The effect of seawater on the macroscopic performance was investigated and analysed based on the results of hydration, microstructure and hydration products of UHPC. The conclusion of this study is summarized as follows:

1. Seawater affected the fresh properties of UHPC. Shortened setting times were observed which was associated with the accelerated hydration by seawater. However, a similar workability in terms of slump flow was observed when using seawater as the mixing water when compared to tap water.
2. Seawater also modified the strength development. The early compressive strength was improved but the later strength was slightly reduced. The improved strength was related to accelerated hydration and finer pore structure. The reduced later strength was attributed to coarser pore structure and shorter MCL and lower PD of the C-S-H.
3. Seawater increased both the autogenous and drying shrinkage of UHPC. The increased autogenous and drying shrinkage were related to the accelerated

hydration and increased volume of pores lesser than 50 nm in UHPC prepared with seawater.

4. The pozzolanic reaction of silica fume was enhanced by the use of seawater. Higher CH consumption and more C-S-H formation were observed in the seawater samples. The increased reactivity contributed to the higher early compressive strength and higher shrinkage of UHPC.
5. The early compressive strength of the seawater UHPC incorporated with PFA was higher while the later strength was comparable to the tap water group. Incorporation of fly ash reduced the shrinkage, but the shrinkage value was still higher than the tap water mixed samples.

Acknowledgement

The study was supported by a grant from the Theme Based Research Scheme of the Research Grants Council of Hong Kong (Project No. T22-502/18-R). The authors also gratefully acknowledge the support of the University Research Facility on Chemical and Environmental Analysis (UCEA) of PolyU.

Reference

[1] P.J. Monteiro, S.A. Miller, A. Horvath, Towards sustainable concrete, Nat. Mater. 16(7) (2017) 698-699.

[2] A. Ahmed, S. Guo, Z. Zhang, C. Shi, D. Zhu, A review on durability of fiber reinforced polymer (FRP) bars reinforced seawater sea sand concrete, Constr. Build. Mater. 256 (2020) 119484.

[3] T. Dhondy, Remennikov, Alex, & Shiekh, M Neaz, Benefits of using sea sand and seawater in concrete: A comprehensive review, Aust. J. Struct. Eng. 20(4) (2019) 280-289.

[4] J. Xiao, C. Qiang, A. Nanni, K. Zhang, Use of sea-sand and seawater in concrete construction: Current status and future opportunities, Constr. Build. Mater. 155 (2017) 1101-1111.

[5] B.H. Menghuan Guo, Feng Xing, Xiaoqing Zhou, Meng Sun, Lili Sui, Yingwu Zhou,, Characterization of the mechanical properties of eco-friendly concrete made with untreated sea sand and seawater based on statistical analysis, Constr. Build. Mater. 234 (2020) 117339.

[6] J. Wang, E. Liu, L. Li, Multiscale investigations on hydration mechanisms in seawater OPC paste, Constr. Build. Mater. 191 (2018) 891-903.

[7] P. Li, W. Li, T. Yu, F. Qu, V.W. Tam, Investigation on early-age hydration, mechanical properties and microstructure of seawater sea sand cement mortar, Constr. Build. Mater. 249 (2020) 118776.

[8] K. Katano, N. Takeda, Y. Ishizeki, K. Iriya, Properties and application of concrete made with sea water and un-washed sea sand, Third international conference on sustainable construction materials and technologies, 2013.

[9] Z. Shi, Z. Shui, Q. Li, H. Geng, Combined effect of metakaolin and sea water on performance and microstructures of concrete, Constr. Build. Mater. 74 (2015) 57-64.

[10] A. Younis, U. Ebead, P. Suraneni, A. Nanni, Fresh and hardened properties of seawater-mixed concrete, Constr. Build. Mater. 190 (2018) 276-286.

[11] F.M. Wegian, Effect of seawater for mixing and curing on structural concrete, IES J. Part A Civ. Struct. Eng. 3(4) (2010) 235-243.

[12] T.J. Qing Xu, Zhengxian Yang, Yilong Ye,, Preliminary investigation of artificial reef concrete with sulphoaluminate cement, marine sand and sea water,, Constr. Build. Mater. 211 (2019) 837-846.

[13] H.Y. Ghorab, M. Hilal, A. Antar, Effect of mixing and curing waters on the behaviour of cement pastes and concrete Part 2: Properties of cement paste and concrete, Cem. Concr. Res. 20(1) (1990) 69-72.

565 [14] T.U. Mohammed, H. Hamada, T. Yamaji, Performance of seawater-mixed
566 concrete in the tidal environment, Cem. Concr. Res. 34(4) (2004) 593-601.
567 [15] J. Teng, T. Jiang, L. Lam, Y. Luo, Refinement of a design-oriented stress–strain
568 model for FRP-confined concrete, J. Compos. Constr. 13(4) (2009) 269-278.
569 [16] A. Zhou, R. Qin, C.L. Chow, D. Lau, Structural performance of FRP confined
570 seawater concrete columns under chloride environment, Compos. Struct. 216 (2019)
571 12-19.
572 [17] P. Richard, M.H. Cheyrezy, Reactive powder concretes with high ductility and
573 200-800 MPa compressive strength, ACI Mater J. 144 (1994) 507-518.
574 [18] ATSM standard C1856/C1856M - 17, Standard Practice for Fabricating and
575 Testing Specimens of Ultra-High Performance Concret, ASTM International,
576 West Conshohocken, PA,, 2018.
577 [19] T. Li, X. Liu, Y. Zhang, H. Yang, Z. Zhi, L. Liu, W. Ma, S.P. Shah, W. Li,
578 Preparation of sea water sea sand high performance concrete (SHPC) and serving
579 performance study in marine environment, Constr. Build. Mater. 254 (2020) 119114.
580 [20] S. Pyo, S.Y. Abate, H.-K. Kim, Abrasion resistance of ultra high performance
581 concrete incorporating coarser aggregate, Constr. Build. Mater. 165 (2018) 11-16.
582 [21] B. Hasanzadeh, F. Liu, Z. Sun, Monitoring hydration of UHPC and conventional
583 paste by quantitative analysis on Raman patterns, Constr. Build. Mater. 114 (2016) 208-
584 214.
585 [22] H. Zheng, J. Lu, P. Shen, L. Sun, C.S. Poon, W. Li, Corrosion behavior of carbon
586 steel in chloride-contaminated ultra-high-performance cement pastes, Cem. Concr.
587 Compos. 128 (2022) 104443.
588 [23] T. Ahmed, M. Elchalakani, A. Karrech, M. Dong, M. Mohamed Ali, H. Yang,
589 ECO-UHPC with High-Volume Class-F Fly Ash: New Insight into Mechanical and
590 Durability Properties, J. Mater. Civ. Eng. 33(7) (2021) 04021174.
591 [24] R. Yu, P. Spiesz, H. Brouwers, Development of an eco-friendly Ultra-High
592 Performance Concrete (UHPC) with efficient cement and mineral admixtures uses,
593 Cem. Concr. Compos. 55 (2015) 383-394.
594 [25] J. Liu, C. Shi, Z. Wu, Hardening, microstructure, and shrinkage development of
595 UHPC: A review, J. Asian Concr. Fed. 5(2) (2019) 1-19.
596 [26] U. Ebead, D. Lau, F. Lollini, A. Nanni, P. Suraneni, T. Yu, A review of recent
597 advances in the science and technology of seawater-mixed concrete, Cem. Concr. Res.
598 152 (2022) 106666.
599 [27] J.-G. Teng, Y. Xiang, T. Yu, Z. Fang, Development and mechanical behaviour of
600 ultra-high-performance seawater sea-sand concrete, Adv. Struct. Eng. 22(14) (2019)
601 3100-3120.

[28] Z. Dong, G. Wu, H. Zhu, X.-L. Zhao, Y. Wei, H. Qian, Flexural behavior of seawater sea-sand coral concrete–UHPC composite beams reinforced with BFRP bars, Constr. Build. Mater. 265 (2020) 120279.
[29] B.-T. Huang, Y.-T. Wang, J.-Q. Wu, J. Yu, J.-G. Dai, C.K. Leung, Effect of fiber content on mechanical performance and cracking characteristics of ultra-high-performance seawater sea-sand concrete (UHP-SSC), Adv. Struct. Eng. (2020) 1369433220972452.
[30] H. Li, N. Farzadnia, C. Shi, The role of seawater in interaction of slag and silica fume with cement in low water-to-binder ratio pastes at the early age of hydration, Constr. Build. Mater. 185 (2018) 508-518.
[31] ATSM standard D1141-98, Standard Practice for the Preparation of Substitute Ocean Water, ASTM International, West Conshohocken, PA,, 2013.
[32] R. Yu, P. Spiesz, H. Brouwers, Mix design and properties assessment of ultra-high performance fibre reinforced concrete (UHPFRC), Cem. Concr. Res. 56 (2014) 29-39.
[33] BS EN1015-3, Methods of test for mortar for masonry. Determination of consistence of fresh mortar (by flow table) The British Standards Institution, UK, 1999.
[34] B.E. 196-3, Methods of testing cement. Determination of setting times and soundness, The British Standards Institution, UK, 2016.
[35] ATSM standard C1698-19, Standard Test Method for Autogenous Strain of Cement Paste and Mortar, ASTM International, West Conshohocken, PA,, 2019.
[36] BS ISO 1920-8, Testing of concrete. Determination of the drying shrinkage of concrete for samples prepared in the field or in the laboratory, 2009.
[37] I. Klur, B. Pollet, J. Virlet, A. Nonat, CSH structure evolution with calcium content by multinuclear NMR, in: P. Colombet, A.-R. Grimmer, H. Zanni, P. Sozzani (Eds.) Nuclear magnetic resonance spectroscopy of cement-based materials, Springer, Berlin, 1998, pp. 119-141.
[38] P. Suraneni, J. Weiss, Examining the pozzolanicity of supplementary cementitious materials using isothermal calorimetry and thermogravimetric analysis, Cem. Concr. Compos. 83 (2017) 273-278.
[39] S.H. Lee, H.J. Kim, E. Sakai, M. Daimon, Effect of particle size distribution of fly ash–cement system on the fluidity of cement pastes, Cem. Concr. Res. 33(5) (2003) 763-768.
[40] Y. Li, J. Bao, Y. Guo, The relationship between autogenous shrinkage and pore structure of cement paste with mineral admixtures, Constr. Build. Mater. 24(10) (2010) 1855-1860.
[41] A.M. Soliman, Early-age shrinkage of ultra high-performance concrete: mitigation and compensating mechanisms, Graduate Program in Civil and Environmental Engineering, The University of Western Ontario, 2011.

[42] N. Thomas, Corrosion problems in reinforced concrete: why accelerators of cement hydration usually promote corrosion of steel, J. Mater. Sci. 22(9) (1987) 3328-3334.
[43] C. Wilding, A. Walter, D. Double, A classification of inorganic and organic admixtures by conduction calorimetry, Cem. Concr. Res. 14(2) (1984) 185-194.
[44] K. Scrivener, R. Snellings, B. Lothenbach, A practical guide to microstructural analysis of cementitious materials, Taylor & Francis Group, Boca Raton, Florida, 2018.
[45] Y. Sun, Y. Zhang, Y. Cai, W.L. Lam, J.-X. Lu, P. Shen, C.S. Poon, Mechanisms on Accelerating Hydration of Alite Mixed with Inorganic Salts in Seawater and Characteristics of Hydration Products, ACS Sustain. Chem. Eng. 9(31) (2021) 10479-10490.
[46] J. Wang, J. Xie, Y. Wang, Y. Liu, Y. Ding, Rheological properties, compressive strength, hydration products and microstructure of seawater-mixed cement pastes, Cem. Concr. Compos. 114 (2020) 103770.
[47] D.L. Kong, J.G. Sanjayan, Effect of elevated temperatures on geopolymer paste, mortar and concrete, Cem. Concr. Res. 40(2) (2010) 334-339.
[48] Z. Wu, K.H. Khayat, C. Shi, B.F. Tutikian, Q. Chen, Mechanisms underlying the strength enhancement of UHPC modified with nano-SiO2 and nano-CaCO3, Cem. Concr. Compos. 119 (2021) 103992.
[49] S.A. Yaseen, G.A. Yiseen, C.S. Poon, Z. Li, Influence of seawater on the morphological evolution and the microchemistry of hydration products of tricalcium silicates (C3S), ACS Sustain. Chem. Eng. 8(42) (2020) 15875-15887.
[50] W. Li, Z. Jiang, M. Lu, W. Long, F. Xing, J. Liu, Effects of Seawater, NaCl, and Na_2SO_4 Solution Mixing on Hydration Process of Cement Paste, J. Mater. Civ. Eng. 33(5) (2021) 04021057.
[51] T. Nochaiya, W. Wongkeo, A. Chaipanich, Utilization of fly ash with silica fume and properties of Portland cement–fly ash–silica fume concrete, Fuel 89(3) (2010) 768-774.
[52] J.-X. Lu, P. Shen, Y. Zhang, H. Zheng, Y. Sun, C.S. Poon, Early-age and microstructural properties of glass powder blended cement paste: Improvement by seawater, Cem. Concr. Compos. 122 (2021) 104165.
[53] P.K. Mehta, P.J. Monteiro, Concrete: microstructure, properties, and materials, 3rd ed., McGraw-Hill2006.
[54] L. Zhang, X. Qian, C. Yu, M. Fang, K. Qian, J. Lai, Influence of evaporation rate on pore size distribution, water loss, and early-age drying shrinkage of cement paste after the initial setting, Constr. Build. Mater. 226 (2019) 299-306.
[55] B. Lothenbach, A. Nonat, Calcium silicate hydrates: Solid and liquid phase composition, Cem. Concr. Res. 78 (2015) 57-70.

678 [56] W. Kunther, S. Ferreiro, J. Skibsted, Influence of the Ca/Si ratio on the
679 compressive strength of cementitious calcium–silicate–hydrate binders, J. Mater. Chem.
680 A 5(33) (2017) 17401-17412.
681 [57] M. Khatibmasjedi, S. Ramanthan, P. Suraneni, A. Nanni, Shrinkage behavior of
682 cementitious mortars mixed with seawater, Adv. Civ. Eng. Mater. 8(2) (2019) 64-78.
683 [58] L. Wu, N. Farzadnia, C. Shi, Z. Zhang, H. Wang, Autogenous shrinkage of high
684 performance concrete: A review, Constr. Build. Mater. 149 (2017) 62-75.
685 [59] Y. Li, J. Li, Capillary tension theory for prediction of early autogenous shrinkage
686 of self-consolidating concrete, Constr. Build. Mater. 53(28) (2014) 511-516.
687 [60] R.A. Cook, K.C. Hover, Mercury porosimetry of cement-based materials and
688 associated correction factors, Constr. Build. Mater. 7(4) (1993) 231-240.
689 [61] L. Teng, M. Valipour, K.H. Khayat, Design and performance of low shrinkage
690 UHPC for thin bonded bridge deck overlay, Cem. Concr. Compos. 118 (2021) 103953.
691 [62] T. Xie, C. Fang, M.M. Ali, P. Visintin, Characterizations of autogenous and drying
692 shrinkage of ultra-high performance concrete (UHPC): An experimental study, Cem.
693 Concr. Compos. 91 (2018) 156-173.
694 [63] S.A. Mangi, A. Makhija, M.S. Raza, S.H. Khahro, A.A. Jhatial, A Comprehensive
695 Review on Effects of Seawater on Engineering Properties of Concrete, Silicon (2020)
696 1-8.
697 [64] F. Lollini, E. Redaelli, L. Bertolini, Investigation on the effect of supplementary
698 cementitious materials on the critical chloride threshold of steel in concrete, Mater.
699 Struct. 49(10) (2016) 4147-4165.
700 [65] C. Page, Ø. Vennesland, Pore solution composition and chloride binding capacity
701 of silica-fume cement pastes, Mater. Struct. 16(1) (1983) 19-25.
702